

Numerical simulation of multiphase flow at fracture intersections

Wenjuan Zhang ^{a *}, Isam Janajreh ^b, Mohammed Al Kobaisi ^a

^a Department of petroleum engineering, Khalifa University of Science and Technology, Abu Dhabi, UAE

^b Department of Mechanical Engineering, Khalifa University of Science and Technology, Abu Dhabi, UAE

Abstract

Various models of simulating immiscible multiphase flow in a simple fracture intersection is compared numerically in this work. The first two models assume that the fractures can be treated as a type of porous media and fluid flow in fractures is therefore governed by Darcy's law. The fractures are either gridded explicitly (equal-dimensional porous fracture model) to account for the fracture intersection or they are simplified as lower-dimensional entities (lower-dimensional porous fracture model) and fracture intersection is eliminated in the computational domain by using the star-delta transformation. Numerical results of equal-dimensional porous fracture model demonstrate that fracture intersection angle and the scale ratio of fracture length to fracture aperture can impact the multiphase flow behavior at fracture intersections but the effects of these factors cannot be captured by the lower-dimensional porous fracture model. A CFD study is then conducted to gain better insight into the problem by solving the Navier-Stokes equation coupled with Volume of Fluid (VOF) method. The results show that viscosity of the two phases can affect flow at the fracture intersection. When the two phases have the same viscosity, the equal-dimensional porous fracture model agrees qualitatively with CFD results but the porous fracture model is much more sensitive to viscosity contrast than what is predicted by CFD simulation.

Keywords: Fracture modeling, Darcy's law, Navier-Stokes equation, volume of fluid

1. Introduction

Modeling fluid flow and transport phenomenon in fractured geological formations is relevant to a number of technical areas such as management of underground water resources, prediction of contaminate transport in waste repository, exploration of geothermal reservoirs and enhanced oil recovery, etc. Many models have been proposed in the past several decades to address the challenges. In the petroleum engineering literature, for example, a widely used model is the dual-porosity model which was originally proposed by Barenblat et al. [1] and subsequently developed by Warren and Root [2]. The dual porosity model was later extended to simulate multiphase flow in naturally fractured reservoirs by Kazemi et al. [3] and Thomas et al. [4]. The dual porosity model conceptualizes the inter-connected fractures and matrix blocks as two overlapping continua. The classical Darcy's law is applied to each continuum and a transfer function is defined to account for mass transfer between the two systems. Other notable variations of the dual porosity model include dual porosity/dual permeability model [5] and multiple interacting continua method [6]. Since these continuum models homogenize the fracture networks as a continuum, they are best applied to reservoirs with dense and well-connected fractures. If the fracture network is sparse and poorly connected, the accuracy of these models will deteriorate.

To model fluid flow in fractures more rigorously, the discrete fracture-matrix (DFM) is gaining popularity thanks to the progress made in fracture characterization technology and the increase in computing power. Geiger et al. [7] modeled multiphase flow in discrete fractures by gridding both fractures and surrounding matrix explicitly with triangular meshes. Because of the large contrast in size between fracture and matrix, very fine meshes are needed around the fractures. A more efficient way is to model the fracture entities as

* Corresponding author. Tel.: +971028208632

Fax: +9876543210; E-mail: wenjuan.zhang@ku.ac.ae

© 2016 International Association for Sharing Knowledge and Sustainability

DOI: 10.5383/ijtee.18.02.004

($n-1$)-dimensional objects embedded in n -dimensional matrix system as is done in [8-11]. Karimi-Fard et al. [12] proposed a control volume discrete fracture model where the discrete fractures are represented as lower-dimensional entity in the physical domain during gridding and then expanded to equal-dimensional object in the computational domain so that modeling fractures can be integrated into existing control-volume finite-difference simulators. Star-delta transformation is then used to eliminate the control volume at fracture intersections. All the fracture branches meeting at the intersection are then connected directly in the computational domain. Strictly speaking, the star-delta transformation is only exact for incompressible single-phase and errors will be incurred for multiphase flow. Moreover, geometric features of the fracture intersection such as intersection angles are lost during the transformation and their effect on flow is ignored. Another thing to be noted is that all the fracture models mentioned above assume that the fractures can be treated as a kind of porous media, which means that fluid flow in fractures can be described by Darcy's law. Absolute permeability of fractures is often estimated by Poiseuille's law of flow between two parallel plates with an effective hydraulic aperture. For multiphase flow, the concept of relative permeability is also used for fractures directly [13]. In theory, fluid flow in fractures is governed by the most general Navier-Stokes equation and to the best of the author's knowledge, no work has been done to assess the validity of treating fractures as porous media for multiphase flow. The purpose of this work is then two-fold. First, we treat the fractures as porous media and investigate the effect of star-delta transformation on multiphase flow at the fracture intersections. Then we solve the Navier-Stokes equation directly and compare the results with the porous media-approach. The rest of the paper is organized as follows: Details of various mathematical models are given in the next section and results with discussions are presented in section 3 while conclusions are given in the last section.

2. Methodology

2.1. Mathematical Models

If the fractures are treated as porous media, immiscible oil-water two phase flow can be described by the following equations:

$$\frac{\partial(\phi\rho_\alpha S_\alpha)}{\partial t} = -\nabla \cdot (\rho_\alpha \mathbf{v}_\alpha) + \rho_\alpha q_\alpha, \alpha = o, w \quad (1)$$

where ϕ is fracture porosity; S_α and ρ_α are saturation and density of phase α , respectively; o and w denote the oil phase and water phase, respectively; \mathbf{v}_α denotes the Darcy velocity of phase α and q_α is volumetric source of phase α . Velocity \mathbf{v}_α is related to the phase pressure gradient by Darcy's law:

$$\mathbf{v}_\alpha = -\lambda_\alpha K \nabla p_\alpha \quad (2)$$

where λ_α is phase mobility and is defined by $\lambda_\alpha = k_{r\alpha}/\mu_\alpha$ and $k_{r\alpha}$ and μ_α are relative permeability and viscosity of phase α , respectively. $k_{r\alpha}$ is usually assumed be functions of phase saturations S_α . K is the absolute permeability tensor of the porous media, and gravity force is neglected here. To close the model, two additional constraints are required:

$$S_w + S_o = 1, \text{ and } p_o - p_w = p_c(S_w) \quad (3)$$

Where oil is assumed to be the non-wetting phase and water is the wetting phase. p_c is the capillary pressure between the two immiscible phases. To solve the model numerically, we adopt the improved implicit pressure and explicit saturation method (IMPES) [14]. Oil pressure and water saturation is chosen as the primary variables and the model is formulated into a pressure equation and a saturation:

$$\begin{aligned} -\nabla \cdot (\lambda_t K \nabla p_o) &= q_t - \nabla \cdot (\lambda_w K \nabla p_c) \\ \phi \frac{\partial S_w}{\partial t} + \nabla \cdot \mathbf{v}_w &= q_w \end{aligned} \quad (4)$$

Where q_t is the total source term and is defined as $q_t = q_o + q_w$. In deriving the above equation (4), the incompressibility of fluid and porous media is assumed.

The Two-point Flux Approximation (TPFA) finite volume method [15] is used to discretize the above equations. Flux of phase α between two control volumes i and j that share a common interface is approximated as follows:

$$Q_{\alpha,ij} = \int_{\Gamma_{ij}} -\lambda_\alpha K \nabla p_\alpha \cdot \hat{\mathbf{n}} dS \approx \lambda_{\alpha,ij} T_{ij} (p_{\alpha,i} - p_{\alpha,j}) \quad (5)$$

Where $\hat{\mathbf{n}}$ is the unit normal vector to the interface Γ_{ij} ; $p_{\alpha,i}$ and $p_{\alpha,j}$ is pressure of control volume i and j , respectively; T_{ij} is static part of transmissibility and $\lambda_{\alpha,ij}$ is the mobility of phase α evaluated on the interface Γ_{ij} . The first-order upstream weighting is used to calculate $\lambda_{\alpha,ij}$. During each time step, the pressure equation is first solved implicitly for pressure at time level $n + 1$ while the saturation value is kept at the old-time level n . Then the water saturation of each cell is updated explicitly. For the method to be stable, the time step for saturation equation must satisfy the Courant–Friedrichs–Lewy (CFL) condition, see [15] for more details.

For the lower-dimensional porous fracture model, fracture intersections are eliminated in the computational domain by using the star-delta transformation. Fig. 1 shows four fracture segments intersecting at the common point 0. The Transmissibility between any of the two fracture segments are evaluated as:

$$T_{ij} = \frac{T_{i0}T_{j0}}{\sum_k T_{k0}} \quad (6)$$

where T_{k0} denotes the transmissibility between k^{th} fracture segment and the intersection node 0. The details of transmissibility calculation can be found in [12].

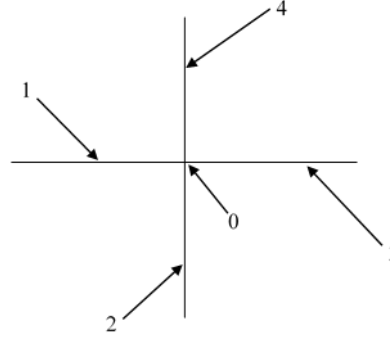


Fig. 1. Star-delta transformation to eliminate fracture intersections

To gain a deeper insight into the multiphase flow behavior at fracture intersections, we further conducted a CFD study using the commercial package Ansys Fluent. The built-in Volume of Fluid (VOF) is chosen to track immiscible oil-water two phase flow. The continuity equation for the volume fraction of each phase takes the following form:

$$\frac{1}{\rho_q} \left[\begin{array}{l} \frac{\partial}{\partial t} (\alpha_q \rho_q) + \nabla \cdot (\alpha_q \rho_q \mathbf{v}_q) = \\ S_{\alpha_q} + \sum_{p=1}^n (\dot{m}_{pq} - \dot{m}_{qp}) \end{array} \right] \quad (7)$$

where α_q is the volume fraction of phase q ; ρ_q is density of phase q and \mathbf{v}_q is velocity of phase q . S_{α_q} is the source term and \dot{m}_{pq} is the mass transfer from phase p to phase q . A single momentum equation is solved throughout the domain:

$$\frac{\partial}{\partial t} (\rho \mathbf{v}) + \nabla \cdot (\rho \mathbf{v} \mathbf{v}) = -\nabla p + \nabla \cdot [\mu (\nabla \mathbf{v} + \nabla \mathbf{v}^T)] + \rho \mathbf{g} + \mathbf{F} \quad (8)$$

where the material properties are calculated by mixing rules. For example, fluid density takes the following form:

$$\rho = \sum_q \alpha_q \rho_q \quad (9)$$

2.2. Results and Discussions

We first compare equal-dimensional porous fracture model with lower-dimensional porous fracture model. The only difference between the two models is that the former model retains the fracture intersections in the computational domain while the latter model eliminates the fracture intersection using star-delta transformation. Two fractures intersect at angle α as is shown in Fig. 2, leading to four fracture branches numbered branch 1, 2, 3 and 4, respectively. Fig. 2 (a) shows the equal-dimensional porous fracture model while the lower-dimensional porous fracture model is shown in Fig. 2 (b). The fracture is assumed to be filled with oil initially and water is injected into the system through the face of branch 1 at constant rate $Q_{inj}=1 \times 10^{-5} \text{ m}^3/\text{s}$. Pressure at the face of branch 2, 3 and 4 are left at atmospheric pressure. All the rest of boundaries are simplified as impenetrable walls. Therefore, the contribution of rock matrix to fluid flow in fractures is ignored. The lengths of the four fracture branches are the same as l and fracture width (aperture) is a . For all the tests presented below, we take a as 1mm. Absolute permeability of fracture is estimated as $k_f = \frac{a^2}{12}$. Viscosity of both water and oil is assumed to be 1 cp.

For equal-dimensional fracture model, triangular meshes are used to mesh the computational domain. Some example meshes are given in Fig. 3. For lower-dimensional fracture model, each fracture branch is discretized by the same number of line segments. The relative permeability of fracture to water and oil takes the usual form of two crossing straight lines as is shown in Fig. 4. Different

fracture intersection angles α and different fracture length/width ratio $\frac{l}{a}$ are tested to investigate the effect of geometry and scale on the transport of multiphase at the fracture intersection. Fig. 5 shows the computational results for the lower-dimensional porous fracture model when the fracture length/width ratio is 10. The relative flow rate (actual flow rate divided by Q_{inj}) of water Q_w and oil Q_o as a function of time for each outlet branch (branch 2, 3 and 4) are recorded. The test results reveal that the flow rate of both water and oil are exactly the same for the three branches and the outflow is evenly distributed among all the outlet branches. Further simulations demonstrate that the results are independent of intersection angle (α) and scale ratio ($\frac{l}{a}$).

Fig. 6 shows the corresponding results of equal-dimensional porous fracture model for different α when l/a is fixed as 10. The left column displays the water and oil flow rate for each outlet branch while the right column shows the total flow rate (water plus oil) for each outlet branch. The results clearly demonstrate that fracture intersection angles can have a significant impact on multi-phase flow behavior at the fracture intersections, especially when the intersection angle is small. It can be observed that outflow is no longer evenly distributed among the three outlet fracture branches. Outlet branch 2 that forms the smallest angle with inlet branch 1 (when $\alpha=30^\circ$ and 60°) has the most amount of flow while the difference of flow rate between branch 3 and 4 is very small. Fig. 7 shows the distribution of water saturation at several time steps and we can see that when the displacing water front reaches the fracture intersection, it moves first into outlet branch 2, which is dictated by the geometry of the fracture intersection. As α increases to approach 90° , the difference of flow rate among the three outlet branches diminishes.

Next, we fix the intersection angle $\alpha=30^\circ$ and increase the scale ratio and run the equal-dimensional porous fracture model. Comparing

Fig. 6 (a) and Fig. 8, we can see that the scale ratio ($\frac{l}{a}$) can also affect flow at the fracture intersection. As the scale ratio increases, the difference of flow rates among the three outlets gradually decreases and approaches the results of lower-dimensional fracture model shown in Fig. 9. The overall results suggest that the lower-dimensional porous fracture model is inadequate to capture the multiphase flow behavior at fracture intersections accurately when the fracture intersection angle and scale ratio is small. However, if the length of fracture is much larger than its aperture, the lower-dimensional porous fracture model can provide a good approximation.

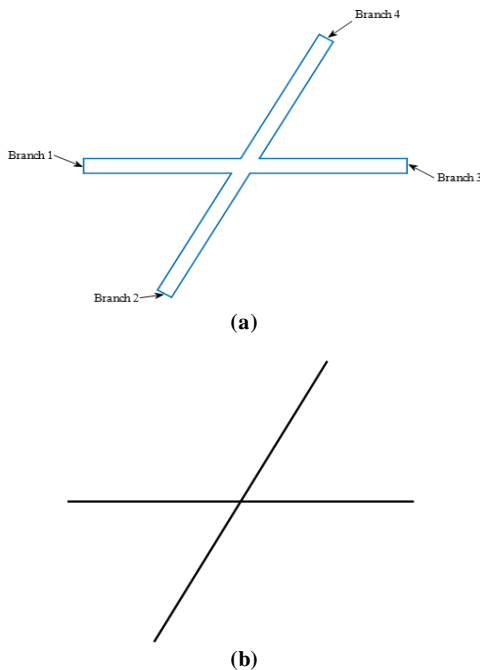


Fig. 2. Equal-dimensional fracture model with four fracture branches (a); corresponding lower-dimensional fracture model with fracture intersection eliminated (b).

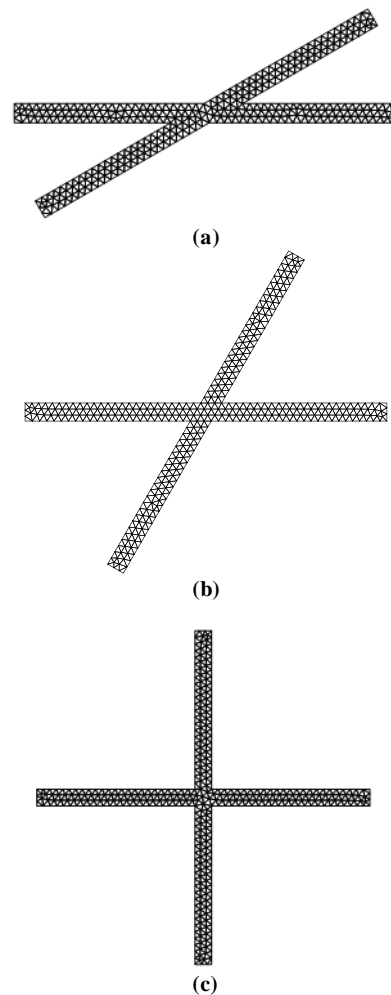


Fig. 3. Triangular meshes for equal-dimensional fracture model with different intersection angles α . From top to bottom: $\alpha=30^\circ$, 60° and 90° .

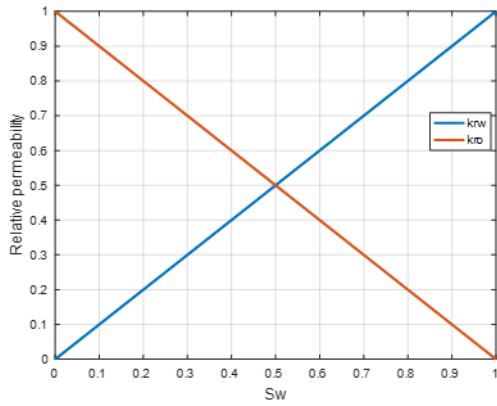


Fig. 4. relative permeability of water (k_{rw}) and oil phase (k_{ro}) as a function of water saturation S_w .

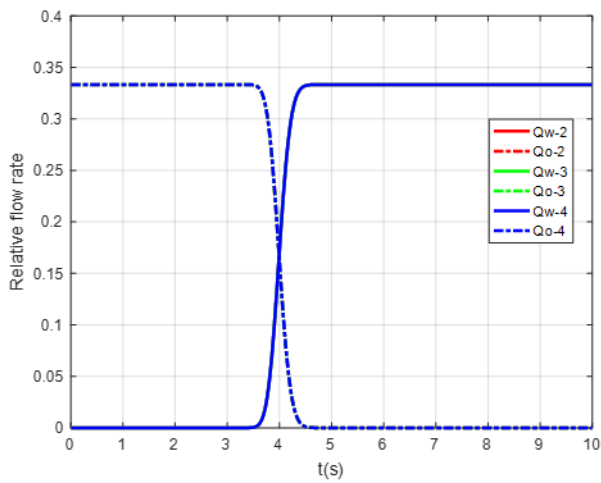
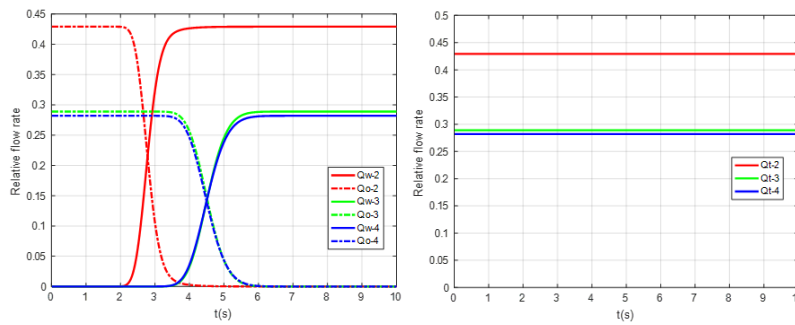
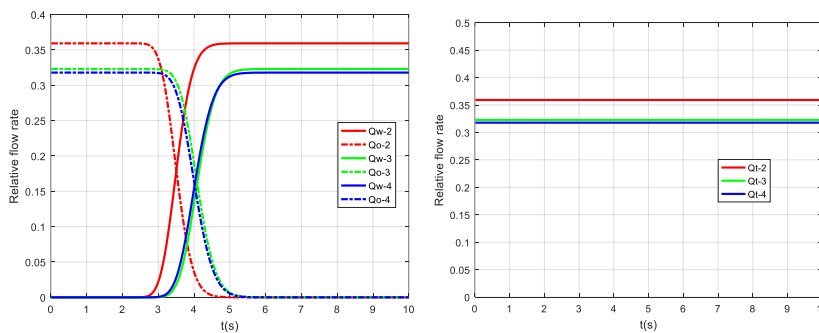


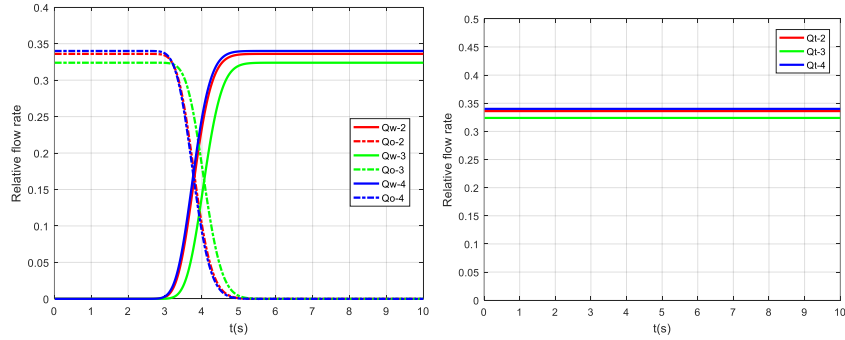
Fig. 5. Oil and water flow rate of each fracture branch for lower-dimensional porous fracture model. $\frac{l}{a} = 10$. The solid lines and dashed lines are overlying one another in the figure, respectively.



(a) $\frac{l}{a} = 10, \alpha = 30^\circ$



(b) $\frac{l}{a} = 10, \alpha = 60^\circ$



(c) $\frac{l}{a} = 10, \alpha = 90^\circ$

Fig. 6. Water, oil flow rate (left column) and total flow rate (right column) of each fracture branch for equal-dimensional porous fracture model with different intersection angles.

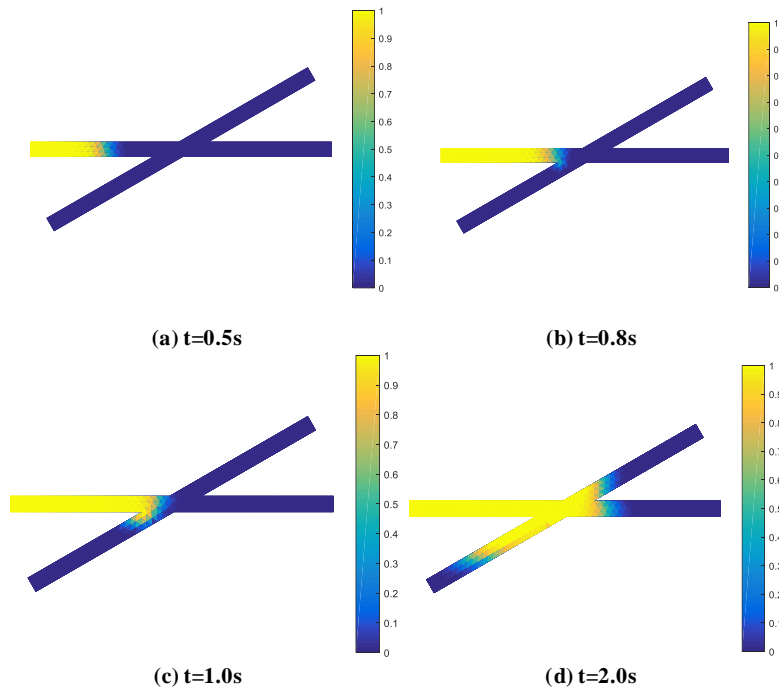
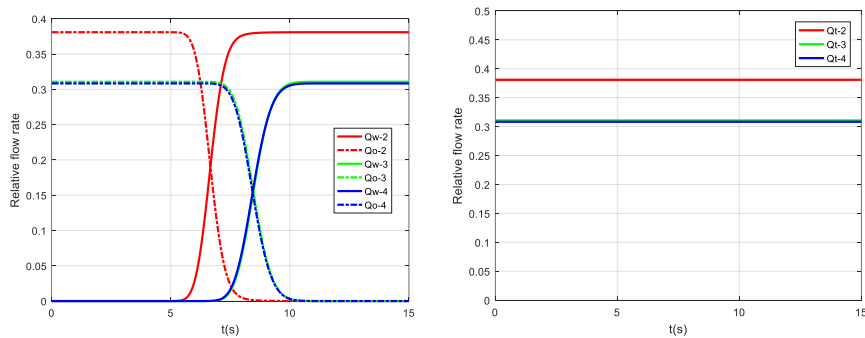


Fig. 7. Distribution of water saturation at different time steps.



(a) $\frac{l}{a} = 20, \alpha = 30^\circ$

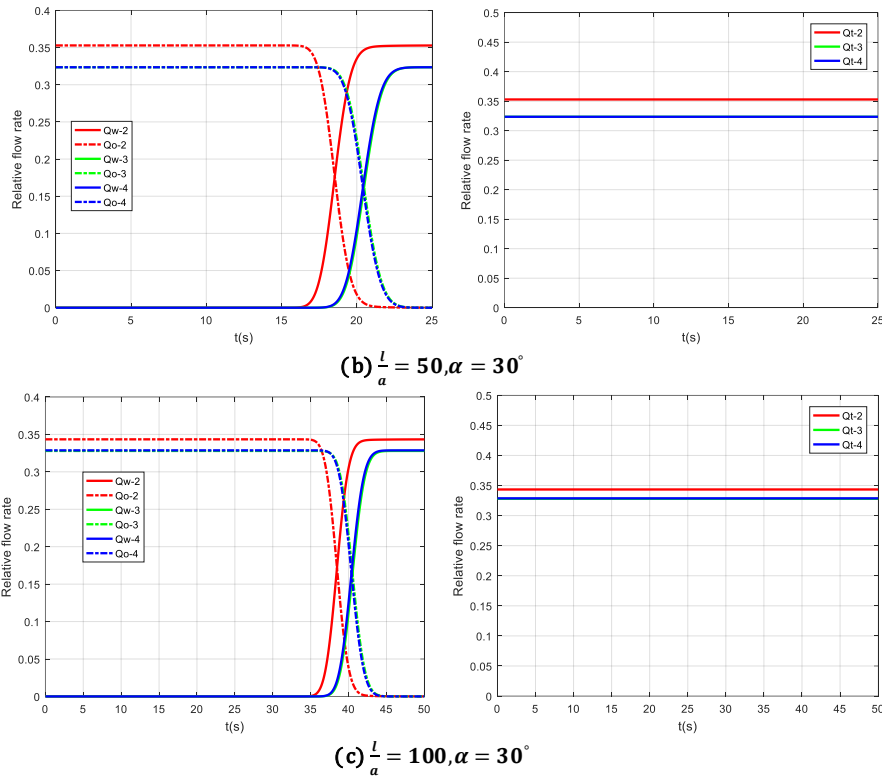


Fig. 8. Water, oil flow rate (left column) and total flow rate (right column) of each fracture branch for equal-dimensional porous fracture model with different scale ratios.

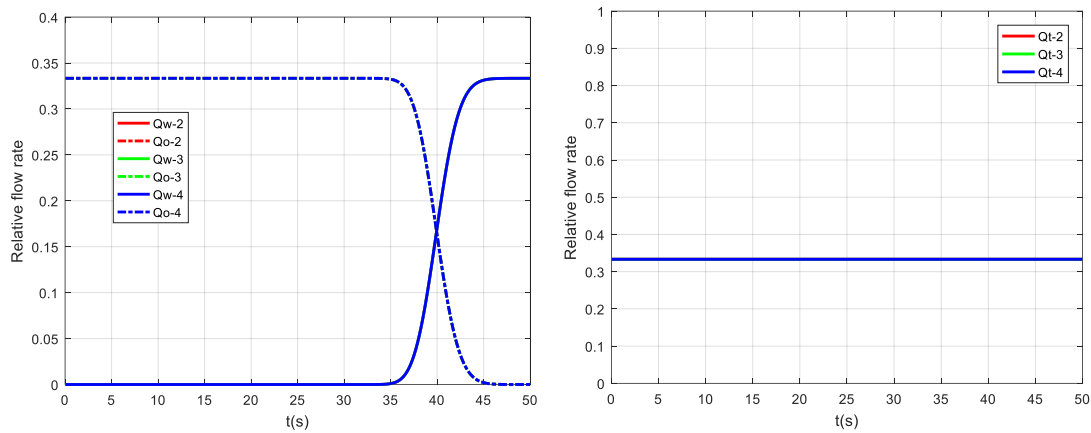


Fig. 9. Water, oil flow rate (left) and total flow rate (right) of each fracture branch for lower dimensional porous fracture model. $l/a=100$

The lower-dimensional and equal-dimensional porous fracture model assumes that the fracture can be treated as a type of porous media and Darcy’s law applies. To gain a deeper insight into the multiphase flow behavior at the fracture intersections, we conducted a computational fluid dynamics (CFD) study by solving the Navier-Stokes equation and employed the volume of fluid (VOF) method to track the oil-water interface. The simulation runs are performed on a commercial CFD package Ansys Fluent. The equal-dimensional fracture model with $\alpha = 60^\circ$ and $\frac{l}{a} = 10$ is used as the computational domain. The set-up of the problem is the same as before except that we change the viscosity ratio of oil to water $\frac{\mu_o}{\mu_w}$ from 0.1, 1 to 10 to

investigate the effect of viscosity contrast on multiphase flow behavior at the fracture intersection. Fig. 10 shows the distribution of volume fraction of water at various time steps for the three cases. From the figure we can see that as the viscosity of oil increases, the displacing water penetrates into the oil more quickly. After the displacing water front reaches the fracture intersection, distribution of water into outlet branches are also affected by the viscosity ratio. For the case of $\mu_o/\mu_w = 0.1$, water is more viscous than oil and it displays a preference to flow straight into fracture branch 3. For the case $\mu_o/\mu_w = 1$ and 10, waters distribute more evenly from the intersection into the 3 outlet branches.

Fig. 11 shows the volume flow rate of both water and oil at each outlet fracture branch for the 3 cases and it can be

seen that more fluid flows through fracture branch 3 than branch 1 and 4, which is in contradiction to the results of equal-dimensional porous fracture model, the results of which is shown in Fig. 12. Considering the simplicity of Darcy's law compared to the full Navier-Stokes equation, we cannot expect the porous fracture model to be able to capture the fluctuations in flow rate displayed in Fig. 11. Therefore, we can only compare the results of porous fracture model with CFD results qualitatively. Fig. 6 (b) and Fig. 11 (b) agrees reasonably well with each other for $\mu_o/\mu_w=1$. However, large discrepancy occurs for the cases of $\mu_o/\mu_w=0.1$ and $\mu_o/\mu_w=10$ as is demonstrated by Fig. 11

(a) and (c) and Fig. 12. Compared to CFD results, the porous fracture model overestimates the time it takes for water to reach the end of outlet fracture branches for the case of $\mu_o/\mu_w=0.1$ but underestimates the time for the case of $\mu_o/\mu_w=10$. For example, the CFD results show that at about 2.5 seconds, water reaches to the end face of all three fracture branches when $\mu_o/\mu_w=10$, but the porous fracture model predicts that this will happen at a much earlier time at less than 0.5 seconds. The simulation results demonstrate that the porous fracture model is much more sensitive to the viscosity ratio between displacing and displaced phases.

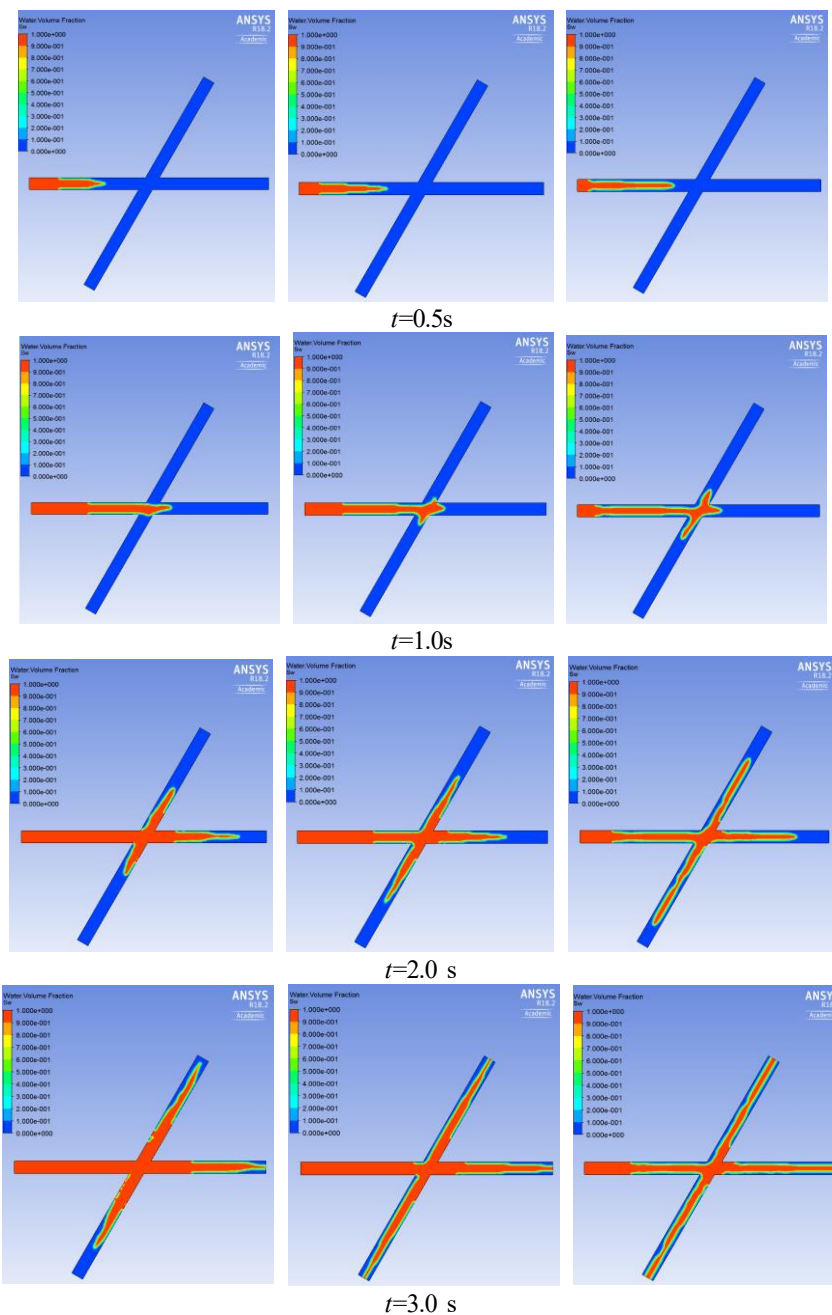


Fig. 10. Distribution of volume fraction of water at different time steps. The three columns correspond to $\mu_o/\mu_w=0.1, 1$ and 10

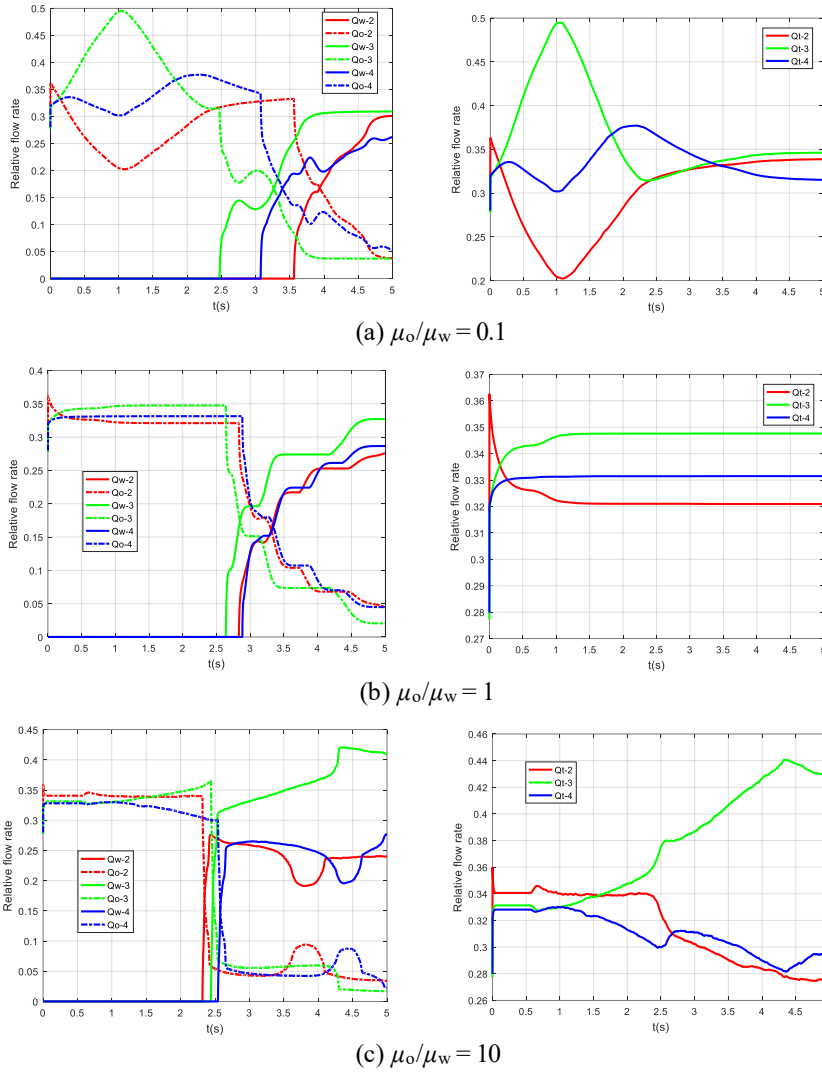


Fig. 11. Water, oil flow rate (left column) and total flow rate (right column) of each fracture branch for 3 different viscosity ratios.

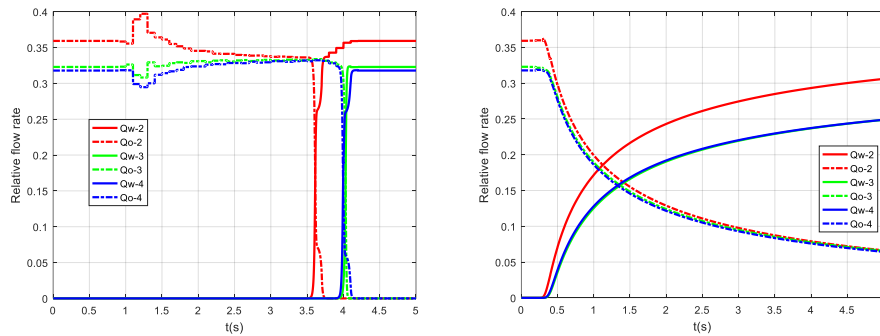


Fig. 12. Water and oil flow rate of each fracture branch for equal-dimensional porous fracture model. Left: $\mu_o/\mu_w=0.1$; right: $\mu_o/\mu_w=10$.

3. Conclusion

In this work numerical experiments are conducted to investigate multiphase flow behavior at fracture intersections. The results of equal-dimensional porous fracture model show that fracture intersection angle (α) and the scale ratio of fracture

length to width (l/a) can affect multiphase flow and transport behavior in the fracture intersection. Specifically, the smaller the angle α and the smaller the scale ratio l/a , the bigger the difference of flow rates among the outlet fracture branches. As α approaches to 90° and/or l/a increases, the difference gradually decreases. The lower-dimensional porous fracture model uses star-delta transformation to eliminate fracture intersection in the computational domain. As a results, the model cannot capture the effect of fracture intersection angle or scale ratio on fluid flow. On the other hand, results of CFD simulation demonstrate that the porous fracture model is much more sensitive to viscosity contrast between the displacing phase and

the displaced phase. When the displacing phase is more viscous, the porous fracture model overestimates the time it takes for the phase to reach the outlet, but the model will give an underestimation when the displaced phase is more viscous.

Acknowledgments

I am grateful to my colleagues in the advanced computational fluid dynamics for their interaction and sharing their thoughts and comments.

References

1. Barenblatt, G.I., I.P. Zheltov, and I.N. Kochina, *Basic concepts in the theory of seepage of homogeneous liquids in fissured rocks [strata]*. Journal of Applied Mathematics and Mechanics, 1960. **24**(5): p. 1286-1303.
2. Warren, J.E. and P.J. Root, *The Behavior of Naturally Fractured Reservoirs*. 1963.
3. Kazemi, H., et al., *Numerical simulation of water-oil flow in naturally fractured reservoirs*. Society of Petroleum Engineers Journal, 1976. **16**(06): p. 317-326.
4. Thomas, L.K., T.N. Dixon, and R.G. Pierson, *Fractured reservoir simulation*. SPEJ, Soc. Pet. Eng. J.:(United States), 1983. **23**(1).
5. Dean, R. and L. Lo, *Simulations of naturally fractured reservoirs*. SPE reservoir engineering, 1988. **3**(02): p. 638-648.
6. Pruess, K. and T. Narasimhan, *Practical method for modeling fluid and heat flow in fractured porous media*. 1982, Lawrence Berkeley Lab., CA (USA).
7. Geiger, S., et al., *Combining finite element and finite volume methods for efficient multiphase flow simulations in highly heterogeneous and structurally complex geologic media*. Geofluids, 2004. **4**(4): p. 284-299.
8. Hoteit, H. and A. Firoozabadi, *An efficient numerical model for incompressible two-phase flow in fractured media*. Advances in Water Resources, 2008. **31**(6): p. 891-905.
9. Ahmed, R., et al., *Three-dimensional control-volume distributed multi-point flux approximation coupled with a lower-dimensional surface fracture model*. Journal of Computational Physics, 2015. **303**(Supplement C): p. 470-497.
10. Ahmed, R., et al., *Control-volume distributed multi-point flux approximation coupled with a lower-dimensional fracture model*. Journal of Computational Physics, 2015. **284**(Supplement C): p. 462-489.
11. Ahmed, R., et al., *CVD-MPFA full pressure support, coupled unstructured discrete fracture–matrix Darcy-flux approximations*. Journal of Computational Physics, 2017. **349**(Supplement C): p. 265-299.
12. Karimi-Fard, M., L.J. Durlofsky, and K. Aziz. *An efficient discrete fracture model applicable for general purpose reservoir simulators*. in *SPE Reservoir Simulation Symposium*. 2003. Society of Petroleum Engineers.
13. Shad, S. and I. Gates, *Multiphase flow in fractures: co-current and counter-current flow in a fracture*. Journal of Canadian Petroleum Technology, 2010. **49**(02): p. 48-55.
14. Chen, Z., *Reservoir simulation: mathematical techniques in oil recovery*. Vol. 77. 2007: Siam.
15. Aarnes, J.E., T. Gimse, and K.-A. Lie, *An Introduction to the Numerics of Flow in Porous Media using Matlab*, in *Geometric Modelling, Numerical Simulation, and Optimization: Applied Mathematics at SINTEF*, G. Hasle, K.-A. Lie, and E. Quak, Editors. 2007, Springer Berlin Heidelberg: Berlin, Heidelberg. p. 265-306.